

Flexural Rigidity of Microtubules and Actin Filaments Measured from Thermal Fluctuations in Shape

Frederick Gittes, Brian Mickey, Jilda Nettleton, and Jonathon Howard

Department of Physiology and Biophysics, and Center for Bioengineering, University of Washington, Seattle, Washington 98195

Abstract. Microtubules are long, proteinaceous filaments that perform structural functions in eukaryotic cells by defining cellular shape and serving as tracks for intracellular motor proteins. We report the first accurate measurements of the flexural rigidity of microtubules. By analyzing the thermally driven fluctuations in their shape, we estimated the mean flexural rigidity of taxol-stabilized microtubules to be $2.2 \times 10^{-23} \text{ Nm}^2$ (with 6.4% uncertainty) for seven unlabeled microtubules and $2.1 \times 10^{-23} \text{ Nm}^2$ (with 4.7% uncertainty) for eight rhodamine-labeled microtubules. These values are similar to earlier, less precise estimates of microtubule bending stiffness obtained by modeling flagellar motion. A similar analysis on seven rhodamine-phalloidin-labeled actin filaments gave a flexural rigidity of $7.3 \times 10^{-26} \text{ Nm}^2$ (with 6% uncertainty), consis-

tent with previously reported results. The flexural rigidity of these microtubules corresponds to a persistence length of 5,200 μm showing that a microtubule is rigid over cellular dimensions. By contrast, the persistence length of an actin filament is only $\sim 17.7 \mu\text{m}$, perhaps explaining why actin filaments within cells are usually cross-linked into bundles. The greater flexural rigidity of a microtubule compared to an actin filament mainly derives from the former's larger cross-section. If tubulin were homogeneous and isotropic, then the microtubule's Young's modulus would be $\sim 1.2 \text{ GPa}$, similar to Plexiglas and rigid plastics. Microtubules are expected to be almost inextensible: the compliance of cells is due primarily to filament bending or sliding between filaments rather than the stretching of the filaments themselves.

MICROTUBULES are proteinaceous filaments that play a central role in cell physiology. In shape, they are hollow cylinders with extreme outer and inner diameters of ~ 30 and 18 nm , respectively, and with lengths of up to $100 \mu\text{m}$ or more. The wall of the cylinder is composed of a regular lattice of the heterodimeric protein tubulin (Amos and Klug, 1974; Beese et al., 1987; Chrétien and Wade, 1991). Microtubules, together with several associated proteins, constitute one of the components of the eukaryotic cytoskeleton: they form the moving cores of cilia and flagella, they are the tracks along which intracellular motor proteins move, and they are thought to define the morphology of many cells. All these roles are structural: they require that microtubules have sufficient resistance to bending. To determine whether microtubules possess appropriate mechanical properties for these cellular functions, we have measured the bending stiffness of purified microtubules in vitro.

We report here the first direct measurements of the flexural rigidity of microtubules. The *flexural rigidity* (EI) or bending stiffness is the quality that describes a filament's resistance to bending forces, just as stiffness describes a filament's resistance to elongation. For a spring, Hooke's law states that force equals stiffness times elongation; for a thin flexible rod, the analogous "beam equation" (Feynman et al.,

1964) states that at each point along the filament the *bending moment* (the torque acting about the point) equals the flexural rigidity times the curvature (the inverse of the radius of curvature). The flexural rigidity of a proteinaceous filament such as a microtubule is completely determined by the properties of the bonds between the atoms within each protein subunit and properties of the bonds which hold the subunits together in the polymer.

In principle, one could directly measure the flexural rigidity by applying a small, known force to one end of a clamped microtubule and measuring its deflection. But, owing to the small size of the microtubule, such a method is technically difficult. We have chosen, instead, to measure the bending of unconstrained microtubules by thermal forces. Thermal bending has been used previously to measure the flexibility of actin filaments, another component of the cytoskeleton. Nagashima and Asakura (1980) and Yanagida et al. (1984) measured the thermal fluctuations of the end-to-end distance of an actin filament; these fluctuations can be related to the filament's flexural rigidity (Landau and Lifshitz, 1980). Unfortunately, microtubules are too rigid to display significant fluctuation in their end-to-end distance, so such measurements on microtubules are not feasible. Furthermore, such measurements lack a test of internal consistency, which is desirable because of the difficulty of distinguishing fluctuations from measurement noise and nonthermal bending. This is crucial for microtubules, which are much stiffer than actin

Address correspondence to J. Howard, Department of Physiology and Biophysics, University of Washington, Seattle, WA 98195.

filaments, and which thus display much smaller fluctuations relative to measurement error. Moreover, for microtubules, even very small convective currents cause bending as large as thermal bending, so that again a consistency check is important.

Our strategy for measuring the flexural rigidity of microtubules was to resolve the thermal bending in a single filament. To do this, we characterized the shape of the filament as the sum of cosine waves (or modes) of increasing frequency: that is, we performed a Fourier decomposition. Each shape that the filament assumed uniquely defined the amplitude of each of the constituent modes. As the filament's shape fluctuated over time due to thermal motions, the amplitude of each mode fluctuated, and the variance of the amplitude of each mode provided an estimate of the flexural rigidity of the filament. Because the amplitude of each mode varied independently of that of the other modes, each mode provided an independent estimate of the flexural rigidity. In practice, we could statistically resolve at most only three modes in a given microtubule. This was sufficient, however, to provide a test of internal consistency: for example, we expect convective flow to affect the different modes to different extents, and so consistent measurements between modes makes it unlikely that the observed bending is due to convective currents. As a further check for systematic error, we compared estimates of flexibility between microtubules of different lengths, and as expected found no dependence.

Along with our analysis of microtubule flexibility, we performed a parallel analysis of the flexural rigidity of actin filaments, in which case as many as four independent modes were analyzed per filament. As in the case of microtubules, the estimates of the flexural rigidity were found to be consistent between modes, and between filaments of different lengths. The results for actin are in general agreement with those of Nagashima and Asakura (1980) and Yanagida et al. (1984).

The mathematical derivations used for the fluctuation analysis are all contained in the Materials and Methods. However, intuitive definitions of all the concepts are contained elsewhere so the paper is readable even if the mathematical sections are skipped.

Materials and Methods

Microtubules

Microtubules were polymerized from thrice-cycled, phosphocellulose-purified tubulin (Weingarten et al., 1974) that was cycled once again before use in order to remove inactive protein (Hyman et al., 1991). Tubulin at 2–6 mg/ml was polymerized by incubation for 30–40 min in 80 mM Pipes, 1 mM EDTA, 5 mM MgCl₂, 1 mM GTP, and 5% DMSO (Aldrich Chemical Co., Milwaukee, WI), pH 6.85, with KOH, at 37°C. The microtubules were stabilized with 10 μ M taxol (Drug Synthesis and Chemistry Branch, Division of Cancer Treatment, National Cancer Institute, Bethesda, MD) to prevent depolymerization and were used within a few hours. The structure of these microtubules is similar to those of microtubules polymerized in the absence of DMSO (Chrétien and Wade, 1991): in a sample of 51 frozen-hydrated microtubules, 20% had 13 protofilaments, 69% had 14, 8% had 15, and 4% had 16 protofilaments. The average number of protofilaments was 14.0, different from the 13 protofilaments found in most, but not all, microtubules inside cells. The microtubules were diluted 100- to 1,000-fold into a solution with final concentrations of 80 mM Pipes, 1 mM EDTA, 1 mM MgCl₂, 10 μ M taxol, and ~0.4–1.0 mg/ml casein to prevent microtubules from adhering to the glass surfaces (unless otherwise indicated, all reagents were obtained from Sigma Chemical Co., St. Louis,

MO). A few microliters of this solution were pipetted onto a clean microscope slide, and a clean cover glass was placed on top; the resulting solution depth of <3 μ m between the surfaces (measured using the calibrated microscope focusing mechanism) effectively constrained the microtubules to move in only two dimensions. The edges of the coverslip were sealed with immersion oil to prevent fluid flow due to evaporation; this was important because even the gentlest flow caused substantial flexure of the microtubules. Nonlabeled microtubules with lengths ranging from 24.5 to 57.2 μ m were observed under a dark-field microscope using a 1.2–1.4 numerical-aperture condenser (Carl Zeiss, Inc., Thornwood, NY) and viewed with a Diastar microscope (Leica, Buffalo, NY). Rhodamine-labeled microtubules (~equimolar tetramethylrhodamine-tubulin and non-labeled tubulin; Hyman et al., 1991) with lengths ranging from 39.1 to 63.2 μ m were observed by fluorescence microscopy; in this case, the buffer was augmented with 0.1 mg/ml glucose oxidase, 0.02 mg/ml catalase, 10 mM D-glucose, and 1% BME (2-mercaptoethanol) to slow photobleaching (Kishino and Yanagida, 1988). All experiments were performed at room temperature (24–26°C). The temperature of shallow aqueous solutions under the same illumination was directly measured using 50- μ m-diameter T-type thermocouple wire (Physitemp Instruments, Inc., Clifton, NJ); the temperature of the filaments under observation was estimated at <1° above

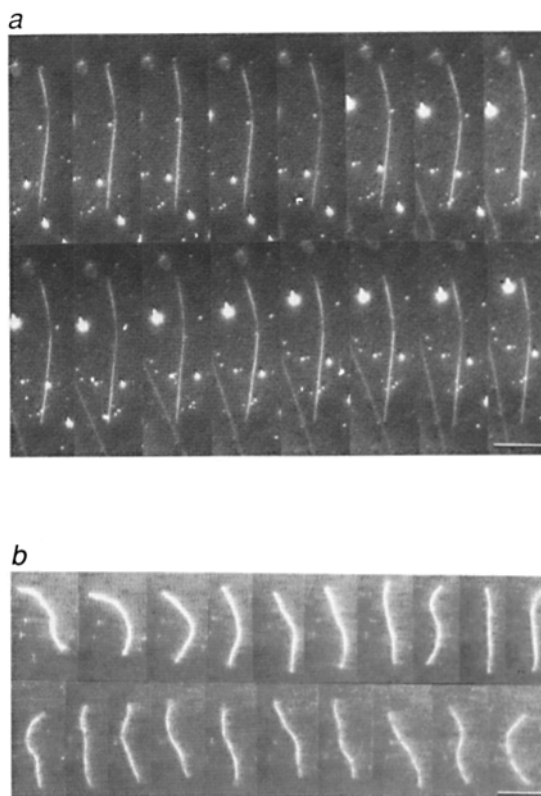


Figure 1. Video images of a microtubule (a) and an actin filament (b) undergoing thermal fluctuations in curvature. The filaments were constrained to move in a very shallow experimental chamber: the chamber depth of <3 μ m prevented the microtubule, which had a large fixed curve, from rotating axially. Each picture in the microtubule collage of dark-field images is separated by 10 s. Each picture in the actin-filament collage of fluorescence images is separated by ~1.5 s. The scale bars represent 10 μ m: the microtubule is 28.9 μ m long, whereas the actin filament is 15.5 μ m long. The fluorescent image in b fades with time due to photobleaching. Due to evanescent scattering, the image intensity along the microtubule is greatest where the filament is most closely apposed to the lower surface. Note that the high rigidity of the microtubule leads to very small fluctuations in curvature; while the fluctuations are clear from the video tapes, the reader must tilt the page to see them in this figure.

ambient temperature; throughout, 25°C is the assumed temperature. Images (Fig. 1) were detected with a silicon-intensified-target camera (Hamamatsu C2400-8; Bartels and Stout, Bellevue, WA) and recorded with a 1/2-inch video cassette recorder (Panasonic AG-6300, Proline, Seattle, WA). Video prints of taped images were made using a Sony UP 5000 video printer.

To record the fluctuating shapes of the microtubules, five to 15 points along the recorded image were digitized from videotape using MEASURE hardware and software (M. Walsh Electronics, San Dimas, CA). The digitized images were corrected numerically for field distortion in the camera. From 51 to 113 such sets of data were acquired at intervals of from 5 to 20 s. This sampling interval was so chosen to ensure that shapes at sequential times were uncorrelated; that is, the sampling time was longer than the relaxation time for any of the modes (see below).

Actin Filaments

Actin filaments were provided by courtesy of Dr. Miklós S. Z. Kellermayer and were prepared as described by Pardee and Spudich (1982). Actin filaments were stabilized against depolymerization with tetramethylrhodamine-isothiocyanate-phalloidin, diluted into buffer (25 mM imidazole-HCl, 2.5 mM KCl, 4 mM MgCl₂, and 1 mM EGTA, titrated with HCl to pH 7.4) augmented with 0.4 mg/ml glucose oxidase, 0.08 mg/ml catalase, 20 mM D-glucose, and 1% BME (2-mercaptoethanol). Additionally, casein was added (<0.5 mg/ml) to prevent actin from sticking to the glass. The actin filaments were observed by fluorescence microscopy. Sequential images of an actin filament undergoing thermal fluctuations is shown in Fig. 1 b. The fluctuating shapes of actin filaments with lengths ranging from 3.7 to 22.7 μm were digitized in the same manner as were the microtubules, and a similar number of sets of data were acquired. A shorter sampling interval of ~0.5 s was used in the case of actin filaments because the fluorescence faded over a few minutes. For the longest actin filaments this sampling time was too short to provide many independent measurements of the lower order, more slowly relaxing modes (see below), but the greater flexibility of the actin filament over the microtubule permitted adequate resolution of higher order modes.

Definition of Flexural Rigidity

If a thin flexible rod of fixed length L is constrained to bend within a plane (i.e., in two dimensions), its shape is completely specified by the tangent angle $\theta(s)$ at every point s along the arc length of the rod ($0 < s < L$). The curvature at each point (i.e., the reciprocal of the radius of curvature) is $d\theta/ds$. If the bending is slight (i.e., the radius of curvature is much greater than the filament diameter as in the cases under study), Hooke's law applies and the flexural rigidity, EI is defined by

$$dU/ds = \frac{1}{2} EI (d\theta/ds - d\theta^0/ds)^2 \quad (1)$$

where dU/ds is the bending energy per unit length and $\theta^0(s)$ is the shape of the relaxed rod in the absence of applied or thermal forces. dU/ds is directly analogous to the energy stored in a spring, $U = 1/2 k(x - x_0)^2$ where k is the stiffness and $x - x_0$ is the extension beyond the spring's natural length, x_0 . The total energy of bending of a thin rod in the plane is

$$U = \frac{1}{2} EI \int_0^L ds (d\theta/ds - d\theta^0/ds)^2. \quad (2)$$

Eqs. 1 and 2, and the concept of flexural rigidity apply microscopically to slightly bent linear molecules even if their molecular structure is complicated.

If the rod is composed of an isotropic elastic substance, EI can be separated as the product of the Young's modulus, E , and the geometrical moment of inertia, I , of the cross-section,

$$I = \iint_{\text{cross-section}} y^2 dA, \quad (3)$$

where y is distance in the direction of the curvature (Landau and Lifshitz, 1986). For a hollow cylinder of inner radius r_i and outer radius r_o ,

$$I = \frac{\pi}{4} (r_o^4 - r_i^4). \quad (4)$$

For the bending of a microtubule or an actin filament, however, the molecular structure is not isotropic, and it is only an approximation to speak of E and I as having independent significance.

Decomposition of Filament Shape into Cosine Modes

We can express the shape $\theta(s)$ as a superposition of a large number of Fourier "modes,"

$$\theta(s) = \sum_{n=0}^{\infty} \theta_n(s) = \sqrt{\frac{2}{L}} \sum_{n=0}^{\infty} a_n \cos\left(\frac{n\pi s}{L}\right). \quad (5)$$

Fig. 2 shows an example of such a decomposition for the case of an actin filament. The choice of cosine "modes" in Eq. 5 is somewhat arbitrary, because no boundary conditions have been imposed on $\theta(s)$. This particular cosine expansion was chosen for computational convenience; a sine or mixed sine and cosine expansion could equally well have been used. The coefficients, a_n do not represent the true dynamical mode amplitudes (see below); nevertheless, the energy of bending U is a simple quadratic sum of these coefficients:

$$U = \frac{1}{2} EI \sum_{n=1}^{\infty} \left(\frac{n\pi}{L}\right)^2 (a_n - a_n^0)^2. \quad (6)$$

Here, a_n^0 denotes the amplitude in the absence of applied or thermal forces and is nonzero if the relaxed filament is not absolutely straight. Note that the zero-order mode (a_0) corresponds to the average orientation of the filament and does not contribute to the bending energy. In equilibrium, the equipartition theorem (Reif, 1965) states that each quadratic term in Eq. 6 contributes an average $1/2 kT$: this implies that for $n \geq 1$,

$$\text{var}(a_n) = \langle (a_n - a_n^0)^2 \rangle = \frac{kT(L)}{EI n\pi^2}. \quad (7)$$

The angle brackets denote an average. The lack of cross-terms in U implies that the quantities $a_n - a_n^0$ are uncorrelated for different n . Thus, the variation, or fluctuation, in amplitude of each mode ($n \geq 1$) provides an independent estimate of the flexural rigidity. In our experiments, the high rigidity of microtubules allowed reliable measurement of only the first three modes. The lower rigidity of actin filaments allowed measurement of up to the sixth mode (a_6).

Definition of Persistence Length L_p

The thermal bending of flexible polymers is commonly discussed in terms of the three-dimensional persistence length $L_p = EI/kT$, which is the arc length above which the angle $\theta(s)$ becomes uncorrelated in three-dimensional motion. Specifically,

$$\langle \cos[\Delta\theta_3(s)] \rangle = \exp(-s/L_p), \quad (8)$$

where $\Delta\theta_3(s)$ is the three-dimensional angle change over the arc length s (Landau and Lifshitz, 1980). Note that when the polymer is constrained to a plane, the decay length is doubled: $\langle \cos[\Delta\theta(s)] \rangle = \exp(-s/2L_p)$, where $\Delta\theta(s)$ is the two-dimensional angle. For slightly flexible rods such as microtubules, the persistence length L_p is much greater than the length of the rod. For actin filaments such as those used in this study, L_p is of the same order of magnitude as the filament length. Using Eq. 7, the persistence length can be written as

$$L_p = \frac{L^2}{n^2 \pi^2 \text{var}(a_n)}. \quad (9)$$

Numerical Estimation of Filament Shape

To find the flexural rigidity EI from Eq. 7, or the persistence length L_p from Eq. 9, we used the following numerical procedure to calculate the Fourier coefficients a_n from a set of digitized two-dimensional coordinates taken along the length of the microtubule. $N + 1$ points, (x_k, y_k) , along the length of the curve were digitized. From these points, we derived the length $\Delta s_k = [(x_{k+1} - x_k)^2 + (y_{k+1} - y_k)^2]^{1/2}$ and tangent angles $\theta_k = \tan^{-1} [(y_{k+1} - y_k)/(x_{k+1} - x_k)]$ of a set of N segments that connect the points (Fig. 2). To calculate

$$a_n = \sqrt{\frac{2}{L}} \int_0^L ds \theta(s) \cos\left(\frac{n\pi s}{L}\right), \quad (10)$$

which is the Fourier inverse of Eq. 5 for $n \geq 1$, we used the approximation

$$a_n \approx \sqrt{\frac{2}{L}} \sum_{k=1}^N \theta_k \Delta s_k \cos\left(\frac{n\pi s_k^{\text{mid}}}{L}\right), \quad n = 1, \dots, N-1, \quad (11)$$

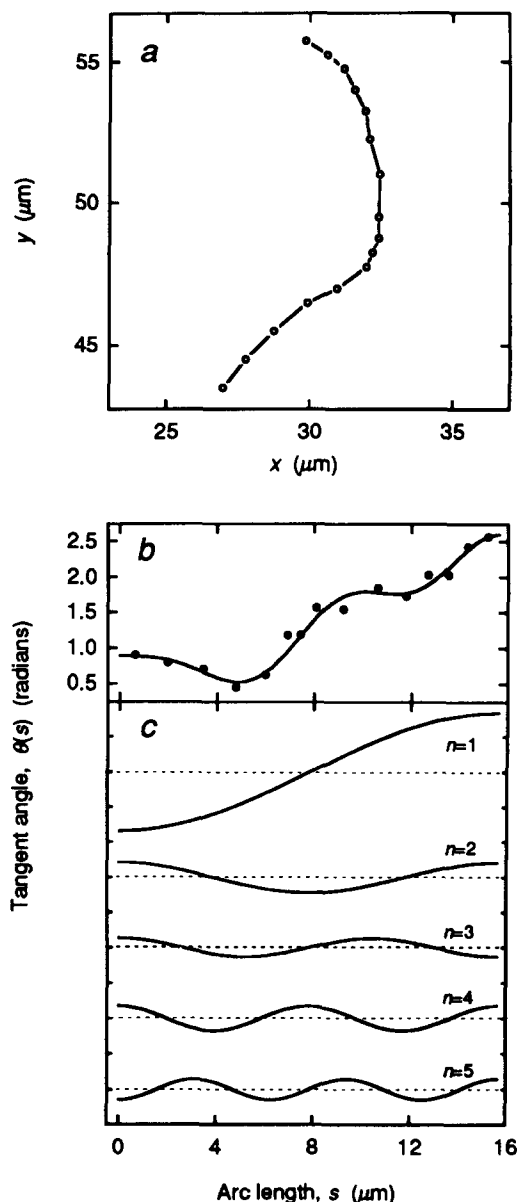


Figure 2. Illustration of the methods by which the images were analyzed. (a) The digitized (x, y) coordinates of 16 points along the length of the actin filament shown in Fig. 1 b, near the time of the first image in that sequence. (b) The tangent angle of each of the segments bounded by the digitized points, plotted against total arc-length up to the midpoint of that segment. (c) Curves showing the first five of the 14 cosine modes into which the tangent-angle curve has been decomposed. The amplitude of each of the cosines was calculated according to Eq. 11. In b, the sum of the first five modes is shown as a solid curve; the sum of all 14 modes would go through each data point. At successive times, the amplitudes of each mode changes as the actin filament shape fluctuates. Because the amplitudes of each mode are statistically independent, the bending energy in each mode will on average be $1/2kT$, and in theory the variance of the amplitude of each mode provides an independent estimate of the flexural rigidity of the filament.

where

$$L = \sum_{k=1}^N \Delta s_k \quad (12)$$

and

$$s_k^{\text{mid}} = \Delta s_1 + \Delta s_2 + \dots + \Delta s_{k-1} + 1/2 \Delta s_k. \quad (13)$$

This procedure is summarized in Fig. 2. In principle, the variance of each of these a_n values as they fluctuate over time may be used to obtain an independent estimate of the flexural rigidity, EI , via Eq. 7. In practice, measurement noise prevents resolution of the higher order modes.

Errors in Estimating the Mode Amplitudes

The experimental estimates of the mode amplitudes obtained via Eq. 11 include errors due to the limited resolution of the microscope and video system: each measured point along the filament deviates from the actual position on the filament by a random distance ϵ_k (Fig. 3). This experimental error, which varies from filament to filament depending on the image quality, adds directly to the true variance of the amplitude of each mode and therefore introduces a bias, not just a random error, into the estimate of EI . Therefore, to obtain an unbiased estimate of the flexural rigidity, the effect of this experimental error must be estimated for each experiment and subtracted from each measured variance. In this section, we derive an approximate expression for the extra variance contributed by the measurement noise: using this expression we are able to estimate the measurement noise for each filament and make the appropriate adjustments.

For small curvatures (the case here), the measurement errors ϵ_k contribute to each a_n independently of the numerical value of a_n itself. To estimate the effect, we can therefore assume that the filament is straight and consider the deviations ϵ_k from a straight line (Fig. 3). As above, let N be the number of segments. For simplicity, we assume all segments have equal length Δs_0 when all the deviations ϵ_k are zero (though in practice the segments had somewhat variable lengths). When the ϵ_k are nonzero, the k^{th} segment has length and angle

$$\Delta s_k = [\Delta s_0^2 + (\epsilon_{k+1} - \epsilon_k)^2]^{1/2} \approx \Delta s_0$$

$$\theta_k = \tan^{-1}[(\epsilon_{k+1} - \epsilon_k)/\Delta s_0] \approx (\epsilon_{k+1} - \epsilon_k)/\Delta s_0 \quad (14)$$

where the orders ϵ_k^2 and higher have been neglected. It follows from Eq. 11 that the errors lead to Fourier-coefficient amplitudes

$$a_n^{\text{noise}} \approx \sqrt{\frac{2}{L}} \sum_{k=1}^N (\epsilon_{k+1} - \epsilon_k) \cos \left[\frac{n\pi}{N} (k - 1/2) \right] \quad (15)$$

where $s_k^{\text{mid}} = (k - 1/2)L/N$ is the midpoint of the k^{th} segment. Note that any correction to the measured length L (see below) will only affect Eq. 15 to higher order in the ϵ_k . The variance, $\langle a_n^2 \rangle^{\text{noise}}$, is now calculated by regrouping the terms on the right-hand side of Eq. 15 in terms of each dis-

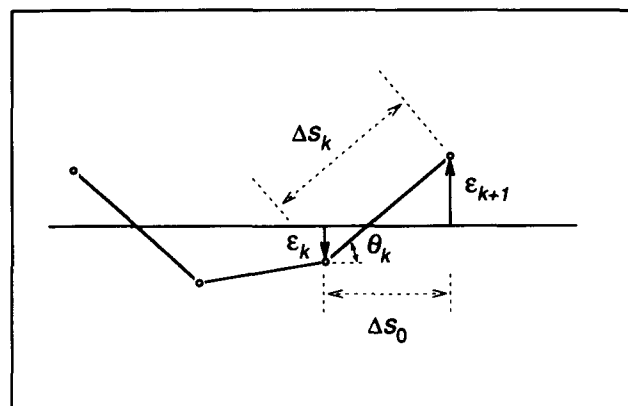


Figure 3. Definitions used in the text to discuss the errors in estimating the mode amplitudes. The hypothetically straight curve is shown as a horizontal line. Points are chosen at an equal horizontal spacing Δs_0 along the curve, but with some vertical error ϵ_k . This results in a nonzero segment angle θ_k , and a segment length Δs greater than Δs_0 .

tinct ϵ_k , then using the fact that the ϵ_k 's are independent, identical random variables, and finally noting that

$$\sum_{k=1}^{N-1} \sin^2\left(\frac{n\pi k}{N}\right) = \frac{N}{2} :$$

$$\langle a_n^2 \rangle^{\text{noise}} = \frac{4}{L} \langle \epsilon_k^2 \rangle \left[1 + (N-1) \sin^2\left(\frac{n\pi}{2N}\right) \right]. \quad (16)$$

This equation predicts how the measurement error contributes to each a_n . In other words, we expect the measured $\text{var}(a_n)$ to be given by

$$\text{var}(a_n)^{\text{measured}} = \left(\frac{L}{n\pi}\right)^2 \frac{1}{L_p} + \frac{4}{L} \langle \epsilon_k^2 \rangle \left[1 + (N-1) \sin^2\left(\frac{n\pi}{2N}\right) \right]. \quad (17)$$

This represents a two-parameter model for comparison with the data where the unknowns are L_p and $\langle \epsilon_k^2 \rangle$. Its form is shown as the solid curves in Fig. 5, a and b : the contribution to the variance from the thermal fluctuations decreases as n increases (Fig. 5, *dashed line*), whereas the contribution from the experimental error increases (Fig. 5, *dotted line*). For each filament, $\langle \epsilon_k^2 \rangle$ was estimated by least-squares curve fitting of $\text{var}(a_n)$ as a function of n (SigmaPlot, Jandel Scientific, Corte Madera, CA). By rearranging Eq. 17 and employing Eq. 16 for $\langle a_n^2 \rangle^{\text{noise}}$, we obtain a modified form of Eq. 9 that provides an almost unbiased (see next section) estimate for the persistence length:

$$\frac{1}{L_p} = \frac{kT}{EI} = \left(\frac{n\pi}{L}\right)^2 [\text{var}(a_n)^{\text{measured}} - \langle a_n^2 \rangle^{\text{noise}}] \quad (18)$$

Error in Estimating the Filament Length

Measurement error also leads to an overestimate of the filament length calculated by Eq. 12, and this overestimate will bias slightly the estimate of persistence length obtained by Eq. 18. Let L' denote the length as measured via Eqs. 12, and L denote the true length. From Eqs. 12 and 14,

$$L' = \sum_{k=1}^N \Delta s_k \cong \sum_{k=1}^N \Delta s_0 \left[1 + \frac{1}{2} \left(\frac{\epsilon_k + 1 - \epsilon_k}{\Delta s_0} \right)^2 \right]. \quad (19)$$

Averaging this expression over the $N + 1$ -independent ϵ_k , and putting $L = N\Delta s_0$, we get to lowest order in $\langle \epsilon_k^2 \rangle$

$$L/L' \cong 1 - \frac{\langle \epsilon_k^2 \rangle}{\Delta s_0^2}. \quad (20)$$

Because we used L' in Eq. 18, L_p is overestimated by a factor $(L/L')^3$, from the explicit L^2 appearing in Eq. 18 and also from a factor $L^{-1/2}$ appearing in a_n (Eq. 11).

For nonlabeled microtubules in dark-field, the average measurement error (estimated by least-square fits of Eq. 17) was $\langle \epsilon_k^2 \rangle^{1/2} = 0.085 \mu\text{m}$, whereas the overall average segment length was $\Delta s_0 \cong 4.5 \mu\text{m}$, so that from Eq. 20 the relative difference $(L - L')/L$ was only 0.04% and was ignored. For the rhodamine-labeled microtubules the error was smaller. For fluorescent actin filaments, $\langle \epsilon_k^2 \rangle^{1/2}$ was $0.126 \mu\text{m}$ and Δs_0 was $1.38 \mu\text{m}$ on average, so the ratio $(L - L')/L$ was 0.8%; this is discussed further in the Results.

Uncertainty in the Measurement of L_p

For each mode of each filament, Eq. 18 provides an unbiased measurement of the persistence length. To check that the measurements are consistent from mode to mode and from filament to filament, it is necessary to estimate the uncertainty in each measurement of L_p .

The quantity $\text{var}(a_n)$ which in our case generally dominates Eq. 18, is expected to be distributed as χ^2_1 ; the uncertainty or standard deviation is therefore

$$\delta \text{var}(a_n) = \text{std}[\text{var}(a_n)]_{M \text{ samples}} \approx \sqrt{\frac{2}{M-1}} \text{var}(a_n), \quad (21)$$

where M is the number of sample values (Box et al., 1978). Because the standard deviation in Eq. 21 is proportional to the mean, and because the distribution of the logarithm, $\ln[\text{var}(a_n)]$, is better approximated by the normal distribution than is $\text{var}(a_n)$ (Box et al., 1978), we performed our statistical analysis on $\ln[\text{var}(a_n)]$ and $\ln(L_p)$, rather than on a_n and L_p .

We lack a precise estimate of the uncertainty in the quantity $\langle a_n^2 \rangle^{\text{noise}}$.

Uncertainty in $\langle a_n^2 \rangle^{\text{noise}}$ should include not only the error of the parameter $\langle \epsilon_k^2 \rangle$ obtained by fitting to the model (Eq. 17), but also the fact that model is inexact. We conservatively assign to $\langle a_n^2 \rangle^{\text{noise}}$ an uncertainty equal to its magnitude:

$$\delta \langle a_n^2 \rangle^{\text{noise}} \approx \langle a_n^2 \rangle^{\text{noise}}. \quad (22)$$

Using these assumptions, and using $\ln(x \pm \delta x) \cong \ln(x) \pm \delta x/x$, we obtain the following uncertainty in $\ln(L_p)$:

$$\ln(L_p) = \ln(L_p^{\text{true}}) \pm \delta \ln(L_p) \approx \ln(L_p^{\text{true}}) \pm \frac{\left\{ \frac{2}{M-1} [\text{var}(a_n)^{\text{measured}}]^2 + [\langle a_n^2 \rangle^{\text{noise}}]^2 \right\}^{1/2}}{[\text{var}(a_n)^{\text{measured}} - \langle a_n^2 \rangle^{\text{noise}}]}. \quad (23)$$

Relaxation Times of Small-Amplitude Hydrodynamic Bending Modes

How long does it take for the shape of a filament to change, and do we wait long enough between samples for successive shapes to be independent? The answer depends on the relaxation times of the dynamical modes. In principle, it is even possible to estimate the flexural rigidity of a filament from these relaxation times. This would provide an independent confirmation of the measurements based on the variances of the amplitudes of the cosine modes. In practice, the exact solution for the dynamics of a polymer is intractable, even in two dimensions (Doi and Edwards, 1986). A more serious drawback from an experimental standpoint is that the solution depends on the hydrodynamic drag from the nearby surface that cannot be accurately measured (Brennen and Winet, 1977). Nevertheless, it is instructive to derive an approximate solution for the hydrodynamic modes (in the limit of very small bending) so that the order of magnitude of our persistence-length measurements can be confirmed.

Our starting point is a relation between the bending moment $M(s)$ and the curvature $d\theta/ds$:

$$EI \frac{\partial \theta}{\partial s} = M(s) \quad (24)$$

(Landau and Lifshitz, 1986). This relation is analogous to Hooke's law for a spring ($kx = F$, where k is the spring constant, x is the extension, and F is the force). We may write the bending moment as an integral of the perpendicular drag force $F_1(s) = -\gamma v_1(s)$, where γ is the perpendicular drag coefficient per unit length of the molecule and $v_1(s)$ is the perpendicular velocity,

$$M(s) = \int_s^L F_1(s')(s' - s) ds'. \quad (25)$$

Differentiating twice with respect to s , we obtain

$$\frac{\partial^2 M(s)}{\partial s^2} = F_1(s) = -\gamma v_1(s) = -\gamma \int_0^s \frac{\partial \theta(s')}{\partial t} ds' \quad (26)$$

where in the last equality we have used a small-angle approximation for $v_1(s)$. Differentiating again and substituting into Eq. 24 we obtain

$$EI \frac{\partial^4 \theta}{\partial s^4} = -\gamma \frac{\partial \theta}{\partial t}. \quad (27)$$

The boundary conditions for an unconstrained filament are that both $\partial \theta / \partial s$ and $\partial^2 \theta / \partial s^2$ vanish at $s = 0$ and $s = L$, which follow from (25) from symmetry under exchange of s for $L - s$. The differential equation is solved by separation of variables to yield the set of decay modes for θ_n :

$$\theta_n(s, t) = \begin{cases} e^{-t/\tau_n} \left[\sinh \alpha_n \sin \frac{2\alpha_n}{L} \left(s - \frac{L}{2} \right) + \sin \alpha_n \sinh \frac{2\alpha_n}{L} \left(s - \frac{L}{2} \right) \right]; & n \text{ odd} \\ e^{-t/\tau_n} \left[\cosh \alpha_n \cos \frac{2\alpha_n}{L} \left(s - \frac{L}{2} \right) + \cos \alpha_n \cosh \frac{2\alpha_n}{L} \left(s - \frac{L}{2} \right) \right]; & n \text{ even} \end{cases} \quad (28)$$

where

$$\tan \alpha_n = (-1)^n \tanh \alpha_n \quad (29)$$

and

$$\tau_n = \frac{\gamma}{EI} \left(\frac{L}{2\alpha_n} \right)^4. \quad (30)$$

The solutions α_n determined by Eq. 29 are closely approximated by the solutions

$$\alpha_n \cong (n + 1/2)\frac{\pi}{2}, \quad n = 1, 2, 3, \dots \quad (31)$$

Therefore, the relaxation times τ_n are approximated by

$$\tau_n \cong \frac{\gamma}{EI} \left[\frac{L}{\pi(n + 1/2)} \right]^4, \quad n = 1, 2, 3, \dots \quad (32)$$

These dynamic modes are connected to our Fourier analysis as follows: as functions of s , each dynamic mode θ_n in Eq. 28 resembles the function $\cos(n\pi s/L)$ in Eq. 5. Each dynamic mode θ_n also has a time-dependent factor e^{-t/τ_n} , i.e., a relaxation time τ_n . Because relaxation times correspond to correlation times of fluctuations (by the fluctuation-dissipation theorem; Landau and Lifshitz, 1980) we can use these τ_n as estimates of correlation times for the fluctuating amplitudes of the modes θ_n and thus, approximately for the fluctuating Fourier amplitudes a_n .

To apply this equation to the microtubules and actin filaments, we use an approximate formula for γ , the perpendicular drag coefficient per unit length of a cylinder near a surface (Brennen and Winet, 1977: $\gamma \cong 4\pi\eta/\ln(2h/r)$, where η is the viscosity ($\eta = 0.89 \times 10^{-3} \text{ kg} \cdot \text{m}^{-1}\text{s}^{-1}$ for water at 25°C), h is the height of the cylinder axis above the surface (taken to be $1 \mu\text{m}$), and r is the hydrodynamic radius of the cylinder. For our longest microtubule, L is $63.2 \mu\text{m}$, r is $\sim 15 \text{ nm}$ and EI is $2.1 \times 10^{-23} \text{ Nm}^2$ (see Results) and Eq. 32 gives a relaxation time of $\tau_1 = 3.9 \text{ s}$ for the first mode. This time is short enough that we should observe no serial correlation with our sample time of 5–20 s, as was in fact the case (Fig. 4 *a*). In the case of actin filaments, the hydrodynamic radius is $\sim 4.5 \text{ nm}$ and our final result for EI is $7.3 \times 10^{-26} \text{ Nm}^2$ (see Results). For our longest actin filament (of length $22.7 \mu\text{m}$) this r and EI give $\tau_1 = 15 \text{ s}$ and $\tau_2 = 2.0 \text{ s}$, showing that with our sample time of 0.5–1.0 s, we would expect to find a large serial correlation in the first mode, and a moderate serial correlation in the second mode. This was in fact the case (Fig. 4 *b*).

Results

Fluctuations in Curvature of Microtubules

We observed the thermal fluctuation in the shape of taxol-stabilized microtubules constrained to move in a shallow experimental chamber with thickness $< 3 \mu\text{m}$: Fig. 1 *a* shows a nonlabeled microtubule visualized by dark-field microscopy. The shallow chamber effectively restricted the movements to two dimensions, conferring upon our experiments two advantages: the entire filament was always in the plane of focus, and the analysis of the shape was greatly simplified. Due to structural defects, microtubules are not perfectly straight, but contain fixed bends (Amos and Amos, 1991b) such as those seen in Fig. 1 *a*. Such intrinsic bends were useful because noticeably bent microtubules could not freely rotate axially in the depth of the chamber: artifactual fluctuations of apparent shape due to such rotations were therefore avoided.

Owing to the great rigidity of microtubules, the fluctuations in their curvature are much smaller than those of the much-less-rigid actin filaments studied in parallel experiments (Fig. 1 *b*). Although the fluctuations in the microtubule of Fig. 1 *a* are readily apparent on the video tapes, the reader must tilt the page to see shape fluctuations from the photographs.

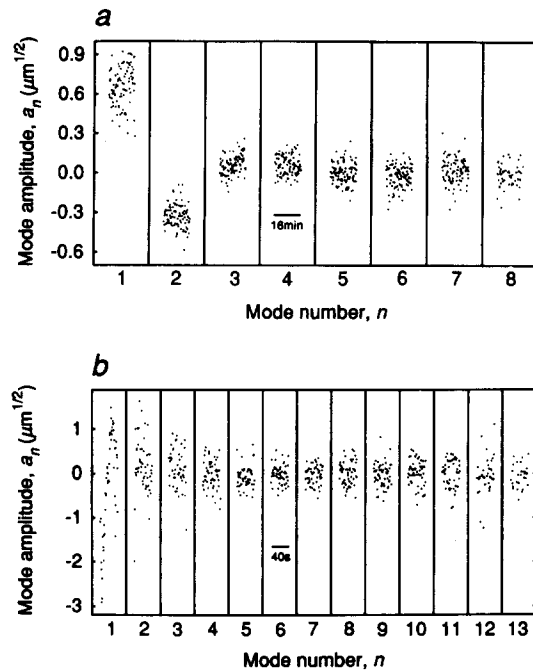


Figure 4. The amplitude of each bending mode of (a) the microtubule shown in Fig. 1 *a* and (b) the actin filament shown in Fig. 1 *b*. The mode amplitude is plotted as a function of time in each of the subpanels (the 16 min of data in *a* excludes an unusable 4-min lacuna). Some times do not have values for the highest modes (largest n) because the number of points digitized was variable. Note that the large fixed bend in the microtubule, apparent in Fig. 1 *a*, shows up as a nonzero mean amplitude in the lowest modes. Information about the flexural rigidity of the filaments is contained in the variance of the mode amplitudes. For both filaments, the lowest modes have a higher variance than the higher modes, whose amplitudes become dominated by experimental noise. The 10-s sampling interval for the microtubule is sufficiently long that successive points are uncorrelated. The 0.5-s sampling interval for the actin filament was too short to prevent correlation for the first mode, as can be seen in the first ($n = 1$) subpanel, but for the higher modes the correlation is negligible. For the microtubule, no statistically significant cross-correlation between the first two modes was measured, as expected by the theory. This rules out the possibility that the variance in these modes is due to microtubule rotation.

To measure the tiny fluctuations of the particular microtubule in Fig. 1 *a*, we decomposed the shape of the microtubule into a sum of cosine modes. In a typical measurement, 10 points along the length of this microtubule were digitized, the lengths and tangent angles of the nine segments between these points were calculated, and then the tangent angle was expressed as a sum of eight cosine waves or modes with amplitudes a_n ($n = 1, \dots, 8$) calculated by Eq. 11. This procedure is illustrated in Fig. 2 which, for clarity, uses not a microtubule but the more flexible actin filament of Fig. 1 *b*. Such measurements were repeated at 10-s intervals for a total of 16 min; the choice of points along the microtubule and their total number were variable. The amplitude of each of the modes for this microtubule is plotted as a function of time in Fig. 4 *a*. The time between measurements was sufficiently long that sequentially acquired amplitudes were uncorrelated, even for the first mode which is the slowest to change

(see Materials and Methods). The large value for the mean of a_1 ($\sim 0.75 \mu\text{m}^{1/2}$) corresponds to the large fixed bend.

The property of interest is not the mean amplitude but the fluctuation about the mean: the vertical width of the clouds of points seen in each of the panels in Fig. 4 *a* is related to the flexural rigidity of the filament. The variance of each a_n about its mean, $\text{var}(a_n)$, is graphed in Fig. 5 *a*. Notice that the variance is different for the different modes. If all the variance were due to measurement noise then we would expect the variance to rise monotonically with n as shown in the dotted line. But this is not the case: the variance starts high, then falls to a minimum before rising again. The excess variance at small n (the lower order modes) is due to bending caused by thermal motions. For these lower order modes, the thermal fluctuations dominate the variance, while for the high order modes the experimental noise dominates. To re-

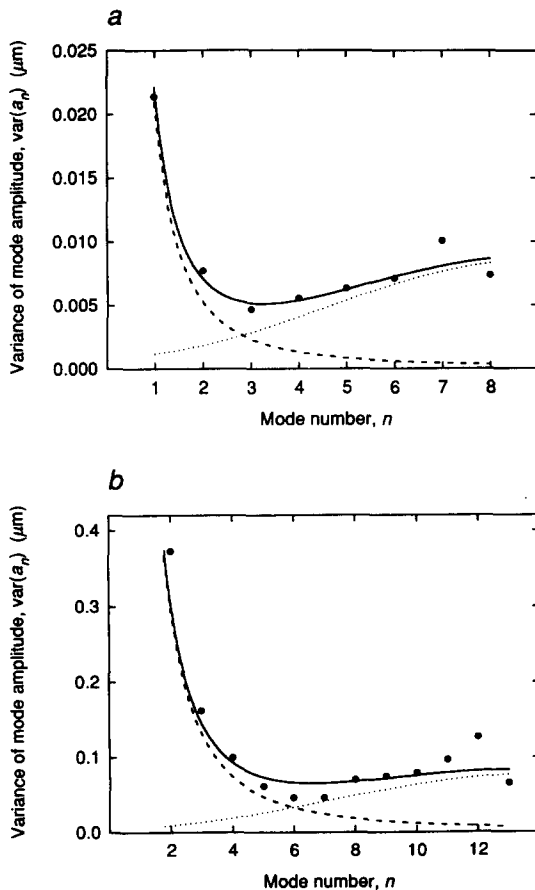


Figure 5. The variance of the Fourier coefficients of each mode plotted against mode number for (a) the microtubule shown in Fig. 1 *a* and (b) the actin filament shown in Fig. 1 *b*. The solid curve is the least-squares fit of Eq. 17 to these variances (with the fit performed on the logarithm of the data, as appropriate for analyzing variances of normally distributed quantities). The estimated variance due to thermal fluctuations in shape is shown by the dashed line, whereas the estimated variance contributed by experimental noise is shown by the dotted line. Thermal fluctuations dominate the variance of the lower modes, while the experimental noise dominates the variance of the higher-order modes. In *b*, the lowest mode ($n = 1$) is not included because strong temporal correlations made its value statistically unreliable.

move the experimental-noise contribution from the variance, we modeled the experimental error [Eq. 17] and performed a least-squares curve fit to the data to estimate its magnitude (Fig. 5, *dotted curve* is experimental noise, and the *dashed curve* is thermal fluctuation). For each mode, the experimental error was subtracted and the flexural rigidity was calculated [via Eq. 18]; only values with a final relative uncertainty of $<50\%$ were used.

In addition to the flexural rigidity we also calculated the persistence length, which is defined as flexural rigidity divided by kT , where k is Boltzmann's constant and T is absolute temperature. The persistence length is a convenient measure of the flexibility because it has a familiar dimension (μm) and is directly proportional to flexural rigidity. The intuitive meaning of persistent length is the length of filament over which the thermal bending becomes appreciable. The actin filament of Fig. 1 *b* has a length approximately equal to its persistence length and the fluctuations in curvature are appreciable, whereas the microtubule of Fig. 1 *a* has a length of $<1\%$ of its persistence length, and so the thermal bends are only very slight.

Flexural Rigidity of Microtubules

The flexural rigidity (and persistence length) measured from seven nonlabeled microtubules and eight rhodamine-labeled microtubules is plotted in Fig. 6 *a*. The data points, whose standard errors were estimated by Eq. 23, include the first three modes of two labeled microtubules, the first two modes of four nonlabeled and five labeled microtubules, and the first mode only of the remaining four microtubules. For both the nonlabeled microtubules and the labeled microtubules, the persistence length was independent of the microtubule length as expected.

The measured flexural rigidity was consistent over all modes and all microtubules. For the seven nonlabeled microtubules, the weighted mean and standard error (Fig. 6, *legend*) of the flexural rigidity was $2.19 \pm 0.14 \times 10^{-23} \text{ Nm}^2$. The extreme deviation from the mean among the 11 data points was 2.3 standard errors; for 11 trials this is expected with probability $P = 0.21$; these data are consistent with each other and with our estimated uncertainties ($P = 0.15$, χ^2 with $d = 10$). The flexural rigidity derived from the seven first-order modes ($2.34 \pm 0.18 \times 10^{-23} \text{ Nm}^2$) was not significantly different ($P = 0.071$) from that derived from the four second-order modes ($1.80 \pm 0.24 \times 10^{-23} \text{ Nm}^2$), yielding no systematic difference between values obtained from the two modes. For the eight rhodamine-labeled microtubules, the mean and standard error were $2.12 \pm 0.10 \times 10^{-23} \text{ Nm}^2$ and again there is no significant deviation of individual mode values from the mean ($P = 0.17$, χ^2 with $d = 16$). Furthermore, the flexural rigidities derived from the eight first-order modes ($2.12 \pm 0.12 \times 10^{-23} \text{ Nm}^2$), the seven second-order modes ($2.33 \pm 0.20 \times 10^{-23} \text{ Nm}^2$); the two third-order modes ($1.57 \pm 0.26 \times 10^{-23} \text{ Nm}^2$) were not significantly different ($P = 0.064$).

Because there was no significant difference in flexural rigidity between the nonlabeled and labeled microtubules, we combined the data to obtain an overall mean of $2.15 \times 10^{-23} \text{ Nm}^2$ (Fig. 6 *a*, *horizontal line*) with a relative uncertainty of 3.8%. This corresponds to a persistence length of $5,200 \pm 200 \mu\text{m}$.

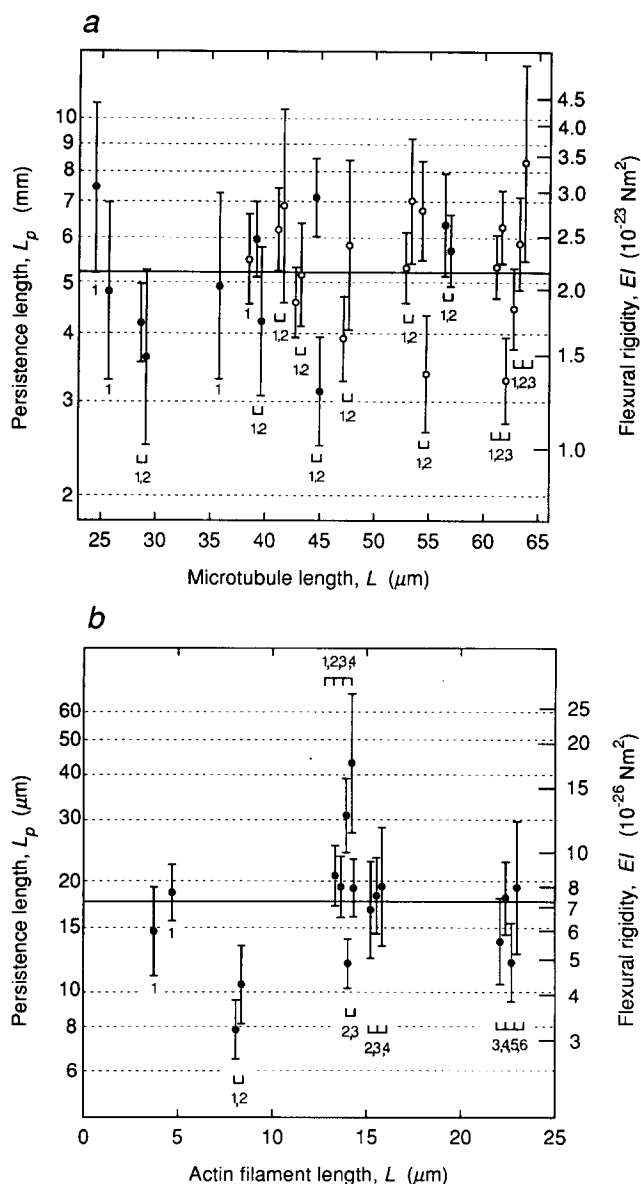


Figure 6. The flexural rigidity (right-hand scale) and persistence length (left-hand scale) are plotted against filament length L for (a) 15 microtubules and (b) seven actin filaments. In both cases, results from different modes of the same filament are separated slightly along the horizontal axis for visibility, and the mode numbers (n values) are indicated above or below the point. In a, the open symbols correspond to rhodamine-labeled microtubules, whereas the closed symbols correspond to nonlabeled microtubules. Note that the vertical scale is a logarithmic one (appropriate for analyzing variances of normally distributed data) which makes the standard errors of each measurement more nearly equal. The horizontal line in a is the mean of the measurements (weighted by the standard errors, with the calculation performed on the logarithms of the data). It corresponds to a flexural rigidity of $2.15 \times 10^{-23} \text{ Nm}^2$, and a persistence length of $5,200 \mu\text{m}$. Because the individual measurements do not significantly deviate from the weighted mean, there is no evidence that we are sampling from a heterogeneous population of microtubules. In b, the lowest mode ($n = 1$) of the actin filament of length $8.1 \mu\text{m}$ gives a value significantly lower than the population average of the other filaments. The horizontal line is the weighted mean of all the modes from the other actin filaments. It corresponds to a flexural rigidity of $7.29 \times 10^{-26} \text{ Nm}^2$, and a persistence length of $17.7 \mu\text{m}$.

As noted above, the overall estimate obtained from the first modes and the overall estimate obtained from the second modes were statistically indistinguishable. Our estimated uncertainties were consistent with the distribution of the data ($P = 0.12$, χ^2 with $d = 27$). Individually, among the 11 first mode-second mode pairs, we found only one case ($L = 44.8 \mu\text{m}$) in which the first and second modes gave significantly different rigidities ($P = 0.040$, 11 trials). Excluding this point did not significantly change the weighted mean, and so we retained it. We do not consider this one value to seriously cast doubt on our assumption that the different modes estimate the same quantity. We also performed a χ^2 analysis and found that at the 95% confidence level, the variation in flexural rigidity of the population of microtubules is $\sim 10\%$ or smaller. Thus, there is no evidence that we are sampling from a heterogeneous population.

Flexural Rigidity of Actin Filaments

A similar analysis was performed for seven rhodamine-phalloidin-labeled actin filaments. The much greater flexibility of the actin filament leads to large fluctuations in shape (Fig. 1 b). These large shape fluctuations obscure any possible intrinsic bends the actin filaments may have. Fig. 4 b shows the mode amplitudes of the particular actin filament in Fig. 1 b; it is apparent that serial correlations exist in the first mode. These correlations make the estimate of flexural rigidity from this mode unreliable. Good estimates from the next three modes of this particular filament were obtained from the variances plotted in Fig. 5 b.

The flexural rigidity and persistence length of seven actin filaments were calculated as described above for microtubules, and are plotted against filament length in Fig. 6 b. As in the case of microtubules, the persistence lengths deduced from different modes were consistent with each other, and independent of actin filament length as expected. The extreme deviation among the 15 values for flexural rigidity was 4.0 standard errors below the mean, occurring in the first mode of the filament of length $8.1 \mu\text{m}$. This is a highly significant deviation ($P < 0.01$). We conclude from this outlying value that the flexural rigidity of our filaments is variable. If we exclude this actin filament, the weighted mean and standard error for the flexural rigidity is $7.29 \pm 0.44 \times 10^{-26} \text{ Nm}^2$, and the persistence length is $17.7 \pm 1.1 \mu\text{m}$.

Evaluation of Sources of Error

When fluctuation analysis is used as a measurement method, particular attention must be paid to experimental errors: experimental errors add to the true variance and therefore introduce bias or systematic error, not just imprecision or random error. To check for systematic errors, we performed three general tests: (a) Were the amplitudes of different modes uncorrelated? (b) Did different modes give consistent estimates for flexural rigidity? (c) Were the flexural rigidities of different microtubules the same and independent of microtubule length? In all three cases, the answer was yes, as expected if no systematic errors were present. We now evaluate the effects of specific sources of error on the measurements.

(a) The most serious noise is due to the random error associated with the digitization of the images-measurement error. The error arises from the limited resolution of the micro-

scope and video apparatus. We modeled this source of variance, estimated its magnitude for each filament (Fig. 5), and subtracted it from the measured variances. Because this variance contributed generally <5% to the variance of the first mode, any residual systematic error arising from this source is certainly <10% of the mean.

(b) The measurement error also leads to an overestimation of the true length of the filament and therefore an overestimation of the persistence length. As discussed after Eq. 20, the bias is negligible for the microtubule measurements, but for the actin filaments the length may be overestimated by as much as $\sim 0.8\%$, leading to an error in flexural rigidity of up to $\sim 2.5\%$. A second effect leads to a small underestimation of the filament length: by partitioning the filament into finite-sized straight-line segments the derived length will be slightly underestimated due to slight bends within the segments. Because the segments were chosen to be much shorter than the persistence lengths ($<10\ \mu\text{m}$ for the microtubules and $<2\ \mu\text{m}$ for the actin filaments), this error will affect the flexural rigidity by $<1\%$.

(c) The nonzero depth of the experimental chamber leads to two types of errors. The smaller is due to the fact that the filament can tilt slightly in and out of the plane of focus; we actually observed and measured the projection of the filament onto the focal plane. Because the persistence length of the microtubules is much greater than the microtubule lengths, little bending occurs in the plane orthogonal to the focal plane, and so the measured length underestimates on average the true length by $1/4(h/L)^2$ where h is the depth of the chamber. For a chamber depth of $\sim 2\ \mu\text{m}$ and microtubule lengths of $>20\ \mu\text{m}$, this effect is smaller than that of (b) above. For the shortest actin filament the length might be underestimated by as much as 7%, and the flexural rigidity underestimated by as much as 23%. The effect on the longer filaments is much smaller.

A potentially large error introduced by a nonzero chamber depth is the artifactual variance caused by free axial rotation of intrinsically bent microtubules. Although the effect is negligible for the actin filaments because their shape fluctuations are much larger than their intrinsic bends, this effect may lead to an underestimate of the true flexural rigidity of microtubules. There are two reasons for thinking that this effect is small. First, such rotation is expected to introduce correlation between the Fourier amplitudes of the modes; no significant correlation was found. Second, the magnitude of the effect depends on the intrinsic shape of the filament via the mean Fourier coefficients a_n^0 : in general these varied from mode to mode and from filament to filament, yet all modes and all filaments gave consistent values for the flexural rigidity.

(d) Another conceivable source of error is torsion: even when intrinsic bends prevent free rotation of microtubules, local twisting of fixed bends may mimic planar bending when viewed from above. However, for elastic rods, the torsional rigidity must be of the same order of magnitude as the flexural rigidity (Landau and Lifshitz, 1986); from this, one finds that over lengths much smaller than the persistence length, the angle of thermal twisting must be very small, and the projection of a rotating bend would hardly change its curvature at all.

(e) Convective currents in the chamber can cause microtubules to bend, especially if they become attached at one

point on the surface. This is one reason why our initial measurements of flexural rigidity on microtubules (Gittes et al., 1992) were 40% smaller than those reported here. In these earlier measurements, the microtubules showed some slight drift. To circumvent this problem, we used immersion oil to seal all the chambers used in this study; under these conditions there was little if any drift. As in the case (c), convective currents are likely to introduce correlations and to affect different modes and different microtubules to different degrees, and no such effects were observed.

(f) The final potential artifact is the possibility that all we are measuring is the fluctuation due to a small number of weak spots along the microtubule that completely dominate the microtubule's compliance: in this case the deduced flexural rigidity would not correspond to a fundamental property of the microtubule's structure. If there existed a small number of such weak spots, their position along the microtubule and their number per microtubule is expected to be quite variable. Thus we would expect that different modes would display different apparent rigidity, and that the flexural rigidity would vary widely from microtubule to microtubule. That this was not the case argues strongly against this possibility.

None of the considerations (b) through (f) should affect our estimate of microtubule rigidity appreciably. In the case of actin filaments, both (b) and (c) may introduce appreciable biases; nevertheless, because these biases are still estimated to be substantially smaller than the experimental uncertainty, we have not attempted to modify our results to compensate for them.

Discussion

By analyzing their thermally driven fluctuations in curvature, we have measured the flexural rigidity, EI , of taxol-stabilized microtubules to be $2.15 \pm 0.08 \times 10^{-23}\ \text{Nm}^2$. The systematic error is likely to be $<10\%$. This flexural rigidity corresponds to a persistence length of $5,200\ \mu\text{m}$. Because the microtubules used in this study had protofilament numbers ranging from 13 to 16 (the most common being 14 [69%] and 13 [20%]; S. Ray, E. Meyhöfer, R. Milligan, and J. Howard, submitted for publication), it may at first seem surprising that we found no evidence that the microtubule population used for this study was heterogeneous. But decreasing the diameter of a microtubule by reducing the protofilament number from 14 to 13 is expected to decrease the flexural rigidity by only about 20% ($\cong 1 - [13/14]^3$ from Eq. 4; the exponent is 3 rather than 4 because the microtubule wall remains the same thickness). This difference is within the experimental error associated with each microtubule. Given the distribution of protofilament numbers, we expect the coefficient of variation of rigidity of the microtubule population to be 0.11, too small to be resolved in our data (see Results).

We should mention earlier studies by Yamazaki et al. (1982) and Mizushima-Sugano et al. (1983) who attempted to measure the persistence length of microtubules assembled from microtubule proteins (tubulin plus microtubule-associated proteins). They estimated the persistence length from measurements of the end-to-end distance. We believe that their values of $79 \pm 30\ \mu\text{m}$ and $73.5 \pm 8.6\ \mu\text{m}$, nearly two orders of magnitude smaller than ours, are gross un-

derestimates due to measurement error. In the first study the variance of their end-to-end distance was independent of the microtubule length, and their persistence length increased linearly with microtubule length; both findings are expected if the variance of the measurement noise is much greater than that originating from thermal fluctuations. In the second study, outlying data points, probably corresponding to intrinsically bent microtubules, may have biased their measurement.

Our measurement of the flexural rigidity of a microtubule is consistent with indirect estimates derived from intact flagella. Computer modeling of the bending of *Ciona* spermatozoa yielded an estimate of 10^{-23} Nm² with an uncertainty of "at least a factor of 2" for the flexural rigidity of the cellular microtubules found in the terminal filament of this flagellum (Omoto and Brokaw, 1982). The flexural rigidity of live echinoderm spermatozoa was directly measured using calibrated glass needles (Okuno and Hiramoto, 1979): the flexural rigidity of the immotile, most-relaxed flagella ranged from 3 to 7×10^{-22} Nm². This agrees with our measurements if three assumptions are made: the nine doublet microtubules in the "9 + 2" array each have two to three times the stiffness of a single microtubule (the central "2" are singlet microtubules); the microtubules are free to slide with respect to each other; and the microtubules dominate the bending stiffness of the relaxed flagellum. Thus, our results lend support to these assumptions.

The similarity between our direct measurements of microtubule flexural rigidity, and indirect measurements obtained from flagellar microtubules in vivo argues that the particular in vitro conditions used for the microtubules in this study—the buffer solution, the taxol used for preventing depolymerization, and the absence of microtubule-associated proteins—do not radically affect the stiffness of the polymer. However, it is possible that microtubule-stabilizing factors such as taxol and microtubule-associated proteins do affect the flexural rigidity. Indeed, preliminary measurements of microtubules in the absence of taxol gave a persistence length between 700 and 1,500 μ m (12 data points; Mickey, B., F. Gittes, and J. Howard, unpublished observations), showing that these unstable microtubules may be less stiff than taxol-stabilized ones.

The flexural rigidity provides an estimate of the load-bearing capacity of microtubules. Our value corresponds to a persistence length of 5.2 mm, much longer than either the microtubules used in this study or the microtubules found in cells. This is consistent with microtubules playing a structural role in defining cell morphology, since microtubules are clearly stable to thermal deformation over cellular dimensions. As an example, our result means (using, e.g., Eq. 2) that ~ 8 kT of work is required to bend a 10- μ m microtubule through an angle of 10°. Another corollary is that a 10- μ m microtubule free to pivot about its end points has a critical buckling force, $F_c = \pi^2 EI/L^2$ (Feynman et al., 1964), of ~ 2 pN, which is of the order of magnitude of the force thought to be exerted by a single motor protein, such as dynein (Kamimura and Takahashi, 1981) or myosin (Bagshaw, 1982; Kishino and Yanagida, 1988). The 24-nm spacing between dynein arms in ciliary axonemes is easily small enough to prevent buckling of the intervening filament.

Knowledge of the flexural rigidity of microtubules permits the estimation of the force exerted by microtubule-based motor proteins in vivo and in vitro. Aist and Bayles (1991) ob-

served buckling of a 7.6- μ m-long mitotic spindle of the fungus *Nectria haematococca* during anaphase B. With our value for the flexural rigidity (corrected for 13 protofilaments), this implies a force of >3.0 pN per microtubule. The force generated by dynein heads in the axoneme can be estimated from the shape of beating spermatozoa. The calculation is somewhat involved because of the complicated geometry of the axoneme. We assume the following: the center-to-center spacing of adjacent doublets is 60 nm (Amos and Amos, 1991a), the average center-to-center spacing projected onto the plane of bending is $w = (2/\pi)60$ nm = 38 nm (Brokaw, 1975), the average spacing of the heads along one doublet is $d = 6$ nm (24 nm for both the outer and inner arms, each arm containing two heads; Amos and Amos, 1991a), the beat amplitude is 4.7 μ m, the beat wavelength measured along the flagellum is 30 μ m (*Ciona*; Brokaw, 1966), and the flexural rigidity of each doublet is $EI = 5 \times 10^{-23}$ Nm² as suggested by the discussion above. We model the dynein activation as an alternating pattern with a fraction $n = 0.5$ of heads active, with all heads active in one half of the axonemal section and none active on the other. We have derived an expression $F = (EId/nw) \partial^2\theta/\partial s^2$ relating force per head F to the rate of curvature change $\partial^2\theta/\partial s^2$; a calculation yields a force per active head of $F = 0.6$ pN. This calculation ignores any passive shear forces between doublets as well as viscous forces acting on the swimming axoneme; it has been calculated that an additional force of ~ 0.18 pN per active head would be required to overcome the viscous force (Brokaw, 1975; counting inner-arm dynein heads). Our estimated force agrees quite closely with the ~ 1 pN force measured from telescoping flagella (Kamimura and Takahashi, 1981). As a third example, we estimate the force exerted by kinesin to buckle microtubules in vitro. Amos and Amos (1991b) observed a microtubule moving across a kinesin-coated surface become stuck at its leading end: the motors at rear produced sufficient force to buckle a 3- μ m section of the microtubule. Because the microtubule segments at each end of the buckle were constrained not to pivot, the buckling force is four times higher than it would be if the ends were free to pivot (Landau and Lifshitz, 1986), and the force exerted by the kinesin motors must exceed 96 pN. Brokaw (1986) deduced comparable forces generated by unspecified motor proteins by using a computer model of the bending of microtubules in squid axoplasm. Because the number of motors is not known, it is not possible to deduce the force per motor.

On a microscopic level, our measurement of EI does accurately reflect the longitudinal compliance of the microtubule lattice. However, we know nothing about the spatial distribution of this compliance within and between the tubulin dimers. Only if the microtubule wall can be described as an elastic continuum do E and I have separate physical meanings. If we make the gross assumption that the microtubule wall is isotropic, our measured value of flexural rigidity implies a Young's modulus, E , of ~ 1.2 GPa. (This estimate uses Eq. 4 to calculate I and assumes that the inner radius corresponds to the "contact radius" measured by Chrétien and Wade [1991] to be 11.48 nm for a 14-protofilament microtubule and that the wall thickness is 2.7 nm, which gives the correct microtubule mass per unit length.) This value for Young's modulus is similar to rigid plastics such as polypropylene or Plexiglas.

For actin filaments, we found the flexural rigidity to be

variable; our best estimate is $EI = 7.29 \pm 0.44 \times 10^{-26}$ Nm², where an aberrant value of $EI = 3.57 \pm 0.54 \times 10^{-26}$ Nm² was excluded. Our measured value for the flexural rigidity of an actin filament corresponds to a persistence length of 17.7 ± 1.1 μ m. These results are in general agreement with previous estimates. Nagashima and Asakura (1980) measured the fluctuation in end-to-end distance and the decay length expressed in Eq. 8; from both measurements performed on actin filaments decorated with myosin and observed by dark-field microscopy in the absence of phalloidin they obtained a persistence length of 12 ± 1 μ m, which increased to 21 ± 2 μ m when tropomyosin was present. We note that this paper contains an erroneous relationship between persistence length and flexural rigidity: we traced this error to Eq. 38 of Harris and Hearst (1966) in which the "3" should be replaced by "2" because there are only 2 degrees of freedom for the angle of a line segment. Yanagida et al. (1984) measured the persistence length of phalloidin-labeled actin filaments to be 15.6 μ m (with no uncertainty reported); decoration by myosin had no consistent effect. Comparison of our results to the earlier studies shows that it is unlikely that the binding of phalloidin drastically altered the flexural rigidity of the filaments.

Unlike microtubules, the cross-section through an actin filament deviates significantly from radial symmetry (Holmes et al., 1990). Therefore the measured value of EI corresponds to the geometric mean of the flexural rigidities measured along the two principal axes of the cross-section (Landau and Lifshitz, 1986). If we model the cross-section of the actin filament as an ellipse with major and minor radii of 3 and 2 nm, respectively (sufficient to incorporate all the protein mass of the filament), and make the gross assumption that the filament is isotropic, we deduce a Young's modulus of 2.6 GPa. Hence, actin filaments are ~ 300 times less resistant to bending than microtubules only because they are thinner and not because actin is more compliant than tubulin. The tubular shape of the microtubule is an economical way to make a rigid structure with a minimum of protein mass: even though the mass per unit length of a microtubule is only ~ 10 -fold higher than that of an actin filament, the microtubule is more than 100 times more resistant to bending. The superior flexural rigidity of microtubules accounts for the observations that microtubules often appear as independent structural elements, whereas actin filaments usually appear in cross-linked bundles such as microvilli, stereocilia, stress fibers and sarcomeres, or in cross-linked networks such as the cell cortex and terminal web.

The Young's moduli for actin and tubulin are similar to the Young's moduli of several other proteinaceous filaments deduced from macroscopic measurements (Wainwright et al., 1976): 5–10 GPa for silk (in *Bombyx mori*), 4 GPa for keratin (in wool), and 0–2.5 GPa for collagen (in rat-tail tendon, where stiffness depends on the strain). These Young's moduli are thousands of times greater than the Young's moduli of rubber-like proteins such as elastin, resilin, and abductin (~ 0.6 MPa). It is perhaps not surprising that microtubules and actin filaments have Young's moduli, which are similar to those of the above tensile proteins; because the principal function of both actin and tubulin is structural, there has probably been evolutionary pressure on both proteins to maximize their mechanical rigidity.

Even though the Young's moduli of microtubules and actin

filaments are only likely to be correct to within an order of magnitude, we can nevertheless draw some strong conclusions regarding the compliance of cells. Dennerll et al. (1988, 1989) used calibrated glass needles to measure the longitudinal stiffnesses (spring constants) of neurites from PC-12 cells and chick dorsal root ganglion cells grown in culture. The mean stiffness was 240 μ Nm⁻¹ for PC-12 cells with neurites of average length ~ 100 μ m. Similar results were obtained for the dorsal root ganglion cells. Each section through a neurite probably contains 10 or more microtubules (Bass et al., 1987), and perhaps as many actin filaments. The question arises: Is the neurite stiffness compatible with the predicted stiffness of the microtubules and actin filaments? The surprising answer is no: the cytoskeletal filaments are much stiffer than the neurite! The stiffness (EA/L) of a single microtubule with length (L) 100 μ m, Young's modulus (E) 1.2 GPa, and cross-sectional area (A) 190 nm² is 2.3 mNm⁻¹, whereas the stiffness of a single, 100- μ m-long actin filament is 470 μ Nm⁻¹ ($E = 2.6$ GPa, $A = 18$ nm²). Thus a single actin filament and a single microtubule are, respectively, two and 10 times stiffer than the entire neurite. This implies that the compliance (the inverse of stiffness) of the cytoskeletal filaments is negligible compared to the compliance of the neurite: in order to accommodate strain, the actin filaments and microtubules cannot be continuous throughout the length of the neurite, and sliding must occur between these filaments. This conclusion is reinforced by the observation that the neurites can be elongated by up to 16%: this is likely to be an order of magnitude greater than the breaking strain of actin filaments (Kishino and Yanagida, 1988) or microtubules. The compliance must originate in other neurite material; if proteins crosslink the cytoskeletal polymers, then these proteins must be highly compliant compared to the cytoskeletal filaments themselves. If neuronal axons in vivo are of similar stiffness to neurites in culture, there is no reason to postulate that neurofilaments, members of the family of intermediate filament proteins which comprise the third component of cytoskeleton, serve purely mechanical roles: the presence of actin filaments and microtubules is expected to provide the axon with ample mechanical rigidity.

In conclusion, we have measured the bending stiffness of taxol-stabilized microtubules and phalloidin-stabilized actin filaments. We believe that this information provides a foundation for the understanding of the dynamic structure of eukaryotic cells. We hope to use knowledge of the flexural rigidity of the cytoskeletal filaments to deduce the force exerted by motor proteins in vitro, and to understand the forces exerted in vivo that result in changes of cell shape.

We thank Sung Baek for technical assistance; Drs. W. Almers, E. Meyerhöfer, and S. Ray; and A. Hunt, E. Munro, and S. Baek for providing helpful comments on the manuscript.

This work was supported by a grant from the National Institutes of Health (AR40593) to J. Howard. Work was performed while J. Howard was a Pew Scholar in the Biomedical Sciences, an Alfred P. Sloan Research Fellow, and was a recipient of the Fondation pour l'Etude du Système Nerveux (FESN) Fellowship on Sensory Transduction. F. Gittes was supported by National Institutes of Health Molecular Biophysics Training Grant GM-08268.

Received for publication 16 July 1992 and in revised form 12 October 1992.

References

- Aist, J. R., and C. J. Bayles. 1991. Detection of spindle pushing forces in vivo during anaphase B in the fungus *Nectria haematococca*. *Cell Motil. Cytoskeleton*. 19:18-24.
- Amos, L. A., and W. B. Amos. 1991a. Molecules of the Cytoskeleton. Guilford Press, New York. 253 pp.
- Amos, L. A., and W. B. Amos. 1991b. The bending of sliding microtubules imaged by confocal light microscopy and negative stain electron microscopy. *J. Cell Sci. Suppl.* 14:95-101.
- Amos, L. A., and A. Klug. 1974. Arrangement of subunits in flagellar microtubules. *J. Cell Sci.* 14:523-549.
- Bagshaw, C. R. 1982. Muscle Contraction. Chapman and Hall, London.
- Baas, P. W., L. A. White, and S. R. Heidemann. 1987. Microtubule polarity reversal accompanies regrowth of amputated neurites. *Proc. Natl. Acad. Sci. USA*. 84:5272-5276.
- Beese, L., G. Stubbs, and C. Cohen. 1987. Microtubule structure at 18 Å resolution. *J. Mol. Biol.* 194:257-264.
- Box, G. E. P., W. G. Hunter, and J. S. Hunter. 1978. Statistics for Experimenters. John Wiley & Sons, Inc., New York. 653 pp.
- Brennen, C., and H. Winet. 1977. Fluid mechanics of propulsion by cilia and flagella. *Annu. Rev. Fluid Mech.* 9:339-398.
- Brokaw, C. J. 1966. Effects of increased viscosity on the movements of some invertebrate spermatozoa. *J. Exp. Biol.* 45:113-139.
- Brokaw, C. J. 1975. Cross-bridge behavior in a sliding filament model for flagella. In *Molecules and Cell Movement*. S. Inoué and R. E. Stephens, editors. Raven Press, New York. 165-179.
- Brokaw, C. J. 1986. Computer simulation of bend propagation by axoplasmic microtubules. *Cell Motil. Cytoskeleton*. 6:347-353.
- Chrétien, D., and R. H. Wade. 1991. New data on the microtubule surface lattice. *Biol. Cell*. 71:161-174.
- Dennerll, T. J., H. C. Joshi, R. E. Buxbaum, and S. R. Heidemann. 1988. Tension and compression in the cytoskeleton of PC-12 neurites II: quantitative measurements. *J. Cell Biol.* 107:665-674.
- Dennerll, T. J., P. Lamoureux, R. E. Buxbaum, and S. R. Heidemann. 1989. The cytomechanics of axonal elongation and retraction. *J. Cell Biol.* 109:3073-3083.
- Doi, M., and S. F. Edwards. 1986. The Theory of Polymer Dynamics. Clarendon Press, Oxford.
- Feynman, R. P., R. B. Leighton, and M. Sands. 1964. The Feynman Lectures on Physics. Vol. II. Addison-Wesley, Reading, MA.
- Gittes, F., B. Mickey, and J. Howard. 1992. The flexural rigidity of microtubules measured from fluctuations of curvature. *Biophys. J.* 62:A27.
- Harris, R. A., and J. E. Hearst. 1966. On polymer dynamics. *J. Chem. Phys.* 44:2595-2609.
- Holmes, K. C., D. Popp, W. Geghard, and W. Kabsch. 1990. Atomic model of the actin filament. *Nature (Lond.)*. 347:44-49.
- Hyman, A., D. Drechsel, D. Kellogg, S. Salser, K. Sawin, P. Steffen, L. Wordeman, and T. Mitchison. 1991. Preparation of modified tubulins. *Methods Enzymol.* 196:478-485.
- Kamimura, S., and K. Takahashi. 1981. Direct measurement of the force of microtubule sliding in flagella. *Nature (Lond.)*. 293:566-568.
- Kishino, A., and T. Yanagida. 1988. Force measurements by micromanipulation of a single actin filament by glass needles. *Nature (Lond.)*. 334:74-76.
- Landau, L. D., and E. M. Lifshitz. 1980. Statistical Physics. 3rd ed., Part I. Pergamon Press, Oxford. 544 pp.
- Landau, L. D., and E. M. Lifshitz. 1986. Theory of Elasticity, 3rd ed. Pergamon Press, Oxford. 187 pp.
- Mizushima-Sugano, J., T. Maeda, and T. Miki-Noumura. 1983. Flexural rigidity of singlet microtubules estimated from statistical analysis of their contour lengths and end-to-end distances. *Biochim. Biophys. Acta*. 755:257-262.
- Nagashima, H., and S. Asakura. 1980. Dark-field microscopic study of the flexibility of F-actin complexes. *J. Mol. Biol.* 136:169-182.
- Okuno, M., and Y. Hiramoto. 1979. Direct measurements of the stiffness of echinoderm sperm flagella. *J. Exp. Biol.* 79:235-243.
- Omoto, C. K., and C. J. Brokaw. 1982. Structure and behaviour of the sperm terminal filament. *J. Cell Sci.* 58:385-409.
- Pardee, J. D., and J. A. Spudich. 1982. Purification of muscle actin. *Methods Enzymol.* 85:164-181.
- Reif, F. 1965. Fundamentals of Statistical and Thermal Physics. McGraw-Hill, New York.
- Wainwright, S. A., W. D. Biggs, J. D. Currey, and J. M. Gosline. 1976. Mechanical Design in Organisms. Princeton University Press, Princeton, NJ.
- Weingarten, M. D., M. M. Suter, D. R. Littman, and M. W. Kirschner. 1974. Properties of the depolymerization products of microtubules from mammalian brain. *Biochemistry*. 13:5529-5537.
- Yamazaki, S., T. Maeda, and T. Miki-Noumura. 1982. Flexural rigidity of singlet microtubules estimated from statistical analysis of fluctuating images. In *Biological Functions of Microtubules and Related Structures*. H. Sakai, H. Mohri, and G. G. Borisy, editors. Academic Press, New York. 41-48.
- Yanagida, T., M. Nakase, K. Nishiyama, and F. Oosawa. 1984. Direct observations of motion of single F-actin filaments in the presence of myosin. *Nature (Lond.)*. 307:58-60.